

# Hierarchical spatial log Gaussian Cox process model for replicated point patterns

Mikko Kuronen<sup>1</sup>, Aila Särkkä<sup>2</sup>, Matti Vihola<sup>3</sup>, and Mari Myllymäki<sup>1</sup>

<sup>1</sup>Natural Resources Institute Finland (Luke)

<sup>2</sup>Mathematical Sciences, Chalmers University of Technology and the  
University of Gothenburg

<sup>3</sup>Department of Mathematics and Statistics, University of Jyväskylä

August 26, 2021

## Abstract

We propose a conditional log Gaussian Cox process (LGCP) model to investigate the effect of a realization  $\mathbf{y}$  of a point process  $Y$  on the intensity of a point process  $X$ . In the motivating forestry example, the point pattern  $\mathbf{y}$  represents large trees and the point pattern  $\mathbf{x}$ , a realization of  $X$ , seedlings. In the model, every point in  $Y$  has a parametric influence kernel or signal, which together form an influence field. Conditionally on the parameters, the influence field acts as a spatial covariate in the (log) intensity of the LGCP model, and the (log) intensity itself is a non-linear function of the parameters. Unlike in the typical unconditional LGCP situation, points of  $Y$  outside the observation window may affect the intensity of  $X$  inside the window. Therefore, we propose a simple edge correction method to account for this edge effect. The parameters of the model are estimated in a Bayesian framework using Markov chain Monte Carlo (MCMC) where a Laplace approximation is used for the Gaussian field of the LGCP model. Since forest data are often measured in small sample plots, we present the estimation procedure based on replicates. The proposed model is fitted to uneven-aged forest stands in Finland to study the effect of large trees on the success of regeneration.

*Key words:* *Bayesian inference, competition kernel, Laplace approximation, MCMC, spatial random effects, tree regeneration*

## 1 Introduction

Let  $X$  and  $Y$  be two point processes in  $\mathbb{R}^2$  representing, e.g., locations of two plant species, where one ( $Y$ ) is affecting the other ( $X$ ) but not vice versa. This kind of hierarchical relationship or interaction occurs often in ecological communities (see e.g. Dieckmann et al., 2000).

The hierarchical interaction assumption affects the inference for  $X$  and  $Y$  greatly since  $Y$  can be modeled independently of  $X$  and  $X$  is modeled conditionally on  $Y$ . A realization of the point process  $Y$  acts then as a source of heterogeneity in the distribution of  $X$ . Höglmander and Särkkä (1999) modeled interaction between two territorial ant species using Gibbs point processes under such an assumption. A similar hierarchical Gibbs point process approach was used in Grabarnik and Särkkä (2009) and Genet et al. (2014). Furthermore, Illian et al. (2009) modeled the spatial pattern of resprouter species ( $X$ ) given the locations of seeders ( $Y$ ) in a hierarchical set-up having an inhomogeneous Poisson process as a model for the resprouters. In our motivating example, modeling the distribution of seedlings ( $X$ ) given the locations of the large trees ( $Y$ ) is of interest. Like in the resprouter and seeder case above, an inhomogeneous Poisson process would be a reasonable model since the effect of large trees could be added in the model as an explanatory variable. However, such a Poisson model is not flexible enough to handle overdispersion caused by some unobserved environmental covariates, other random mechanisms, or replicates. Therefore, we propose a conditional version of the log Gaussian Cox process (LGCP) (Møller et al., 1998) to model the point process  $X$  given a realization of  $Y$ .

In this paper, we concentrate on modeling the effect that  $Y$  has on  $X$ . We assume that each point  $y \in Y$  emits a signal or impulse whose strength decreases with distance from  $y$ . These individual signals are superimposed to form an influence field, which describes the overall influence of the points of  $Y$  on any location  $s$  in the observation window  $W$ . Similar models from ecological field theory have been used to model competition between individuals (Wu et al., 1985; Miina and Pukkala, 2002; Illian et al., 2008). In addition, in spatio-temporal individual-based models, the random field obtained by superimposing the individual signals has been used to describe the overall interaction structure (see e.g. Pommerening et al., 2011). Our idea here is to include the superimposed individual signals in the intensity function of the LGCP model. Using parametric models for the signals, the intensity of the conditional LGCP is a non-linear function of the model parameters. We construct a Bayesian inference approach, where we sample the influence field and other model parameters using Markov Chain Monte

Carlo (MCMC) with an adaptive scheme (Vihola, 2012) and use the Laplace approximation to treat the latent Gaussian random field of the LGCP model.

Typically, there is no need to add an edge correction in the inference of LGCP models (see e.g. Møller and Waagepetersen, 2003). However, an edge correction is needed in the conditional case since the points of  $Y$  outside but near the boundary of the observation window  $W$  may affect the distribution of  $X$  within  $W$ . Based on the assumption that  $Y$  is a Poisson process, we propose a relatively simple edge correction method similar to the one in Kühlmann-Berenzon et al. (2005), which can efficiently be implemented in the MCMC approach. The performance of the edge correction and its robustness with respect to the Poisson assumption of  $Y$  are illustrated in a small simulation experiment.

Finally, the conditional LGCP model is fitted to the motivating forestry data to study how the intensity of new seedlings in a spruce-dominated uneven-aged (boreal) forest is affected by large trees. Our data consist of seven sample plots in two different areas in Southern Finland. The plots in the same area are treated as independent replicates.

The rest of the paper is organized as follows. In Section 2, we give some examples of influence kernels and introduce the conditional LGCP model. The Bayesian estimation approach including the edge correction is described in Section 3. Section 4 presents the results of a simulation experiment that was conducted to explore the performance of the proposed estimation method and especially, of the edge correction method. Finally, the conditional LGCP model is fitted to the forestry data with replicates in Section 5. Section 6 is for discussion.

## 2 Conditional log Gaussian Cox process model

Let us have a bivariate point process in  $\mathbb{R}^2$  consisting of an unmarked point process  $X$  and a marked point process  $Y$ . Let us further assume that we have observed a realization of process  $X$ , namely  $\mathbf{x} = \{x_i\}$ , in a bounded window  $W \subset \mathbb{R}^2$ . Our primary interest is in the spatial pattern  $\mathbf{x}$  which is affected by the spatial pattern  $\mathbf{y} = \{[y_j; m_j]\}$ , which is a realization of  $Y$ . In our motivating example, the aim is to model the spatial configuration of seedlings given the locations (and sizes) of the large trees, and therefore, it feels natural to model the effect of  $\mathbf{y}$  on  $\mathbf{x}$  by using influence kernels around the points of  $\mathbf{y}$ . The pattern of seedlings  $\mathbf{x}$  is typically clustered and, omitting the effect by the large trees  $\mathbf{y}$ , could be modeled by a LGCP (Møller et al., 1998). Below, we give some examples of influence kernels in

Section 2.1 and propose how they can be included in the LGCP model in Section 2.2. Replicated point patterns are discussed in Section 2.3.

## 2.1 Influence kernels and influence field

We assume that each point of the process  $Y$  introduces an influence kernel around its location  $y_j$ , the size of which may depend on the mark  $m_j$  of the point  $y_j$ . The influence kernel  $c(h; \boldsymbol{\theta}_I)$  or  $c(h, m; \boldsymbol{\theta}_I)$ , where  $\boldsymbol{\theta}_I$  is a parameter vector, is typically assumed to decrease with the distance  $h = \|s - y_j\|$  between the location  $s$  of interest and the point  $y_j$ . The mark  $m_j$  may affect the strength and/or the range of the influence kernel. Two simple parametric forms for the influence kernel are

$$c(h; \theta) = \mathbf{1}(h \leq \theta) \quad (1)$$

and

$$c(h; \theta) = \exp(-(h/\theta)^2), \quad (2)$$

where  $\theta > 0$  is an unknown influence range parameter. In (1), each point of  $Y$  has a constant effect within its "zone of influence" (ZOI), and in (2), the influence of a point gradually decreases with the distance from the point according to a Gaussian kernel centered at the point in question and having a range parameter  $\theta$ . Other kernels have been suggested in the literature for different applications, see e.g. Adler (1996); Illian et al. (2008); Pommerening et al. (2011); Pommerening and Maleki (2014); Schneider et al. (2006).

If  $Y$  is a marked point process, i.e. we have some additional information on the points of  $Y$ , it can be meaningful to include the mark information in the influence kernels. For example, the ZOI can increase with the mark (e.g. Pommerening and Maleki, 2014). A marked generalization of (1) can be written as

$$c(h, m; \boldsymbol{\theta}_I) = \mathbf{1}(h \leq f(m; \boldsymbol{\theta}_I)), \quad (3)$$

where the function  $f : \mathbf{R}_+ \rightarrow \mathbf{R}_+$  determines the form of influence. A marked generalization of (2) is given by

$$c(h, m; \boldsymbol{\theta}_I) = m^\alpha \exp\left(-\left(\frac{h}{\theta m^\delta}\right)^2\right) \quad (4)$$

with  $\boldsymbol{\theta}_I = (\theta, \delta, \alpha)$ , where  $\theta > 0$ ,  $\delta > 0$ , and  $\alpha \geq 0$ . If  $\alpha = 0$ , only the range of influence is affected by the mark and if  $\alpha > 0$ , both the range and the strength are affected by it (see e.g. Pommerening et al., 2011).

The influence field of the process  $Y$  can then be defined as a superposition of the individual influence kernels, either additively (shot-noise field)

$$C(s; \boldsymbol{\theta}_I, Y) = \sum_{[y_j, m_j] \in Y} c(\|s - y_j\|, m_j; \boldsymbol{\theta}_I)$$

or following the max-rule (max-field or binary field)

$$C(s; \boldsymbol{\theta}_I, Y) = \max_{[y_j, m_j] \in Y} c(\|s - y_j\|, m_j; \boldsymbol{\theta}_I).$$

While in the first case, the signals are accumulated, the max-field is based on the assumption that only the largest influence matters. Note also that if the influence is binary, e.g. (1) or (3), the max-field is binary as well and there are two phases in  $W$ , influence and influence-free zones. Penttinen and Niemi (2007) considered a random-set generated Cox process based on such a field. In this paper, we only consider the shot-noise fields.

## 2.2 Conditional model

As mentioned above, in the absence of  $\mathbf{y}$ , a LGCP, where the log intensity surface is a Gaussian process, would be a reasonable model for the clustered pattern  $\mathbf{x}$ . However, since  $\mathbf{x}$  is affected by  $\mathbf{y}$ , we introduce a conditional point process model for  $\mathbf{x}$  given  $Y = \mathbf{y}$ , where the intensity of  $X$  is affected by the influence field of  $\mathbf{y}$ . This conditional model is a LGCP with the intensity

$$\Lambda(s; \boldsymbol{\beta}, \boldsymbol{\theta}_I, \mathbf{y}, Z) = \exp(\beta_0 + \beta_1 C(s; \boldsymbol{\theta}_I, \mathbf{y}) + Z(s)), \quad (5)$$

where  $C(s; \boldsymbol{\theta}_I, \mathbf{y})$  is a parametric influence field,  $\boldsymbol{\beta} = (\beta_0, \beta_1)$  and the unknown coefficients  $\beta_0 \in \mathbb{R}$  and  $\beta_1 \in \mathbb{R}$  are the intercept and the strength of the influence field, respectively. If  $\beta_1 < 0$ ,  $\mathbf{y}$  affects the intensity of  $X$  negatively and the influence field  $C(s; \boldsymbol{\theta}_I, \mathbf{y})$  can be interpreted as a thinning of the LGCP process with intensity  $\Lambda(s) = \exp(\beta_0 + Z(s))$ . If, however,  $\beta_1 > 0$ ,  $\mathbf{y}$  has a positive effect on the intensity of  $X$  and there are more points of  $X$  in areas with a high value of  $C(s; \boldsymbol{\theta}_I, \mathbf{y})$ . Furthermore,  $Z := \{Z(s) : s \in \mathbb{R}^2\}$  is a zero-mean stationary Gaussian random field with a covariance function  $C_Z(r; \boldsymbol{\theta}_Z)$  and independent of the influence field. In our application below, we use the Matérn covariance function

$$C_Z(r; \boldsymbol{\theta}_Z, \nu) = \sigma_Z^2 \frac{2^{1-\nu}}{\Gamma(\nu)} \left( \sqrt{2\nu} \frac{r}{\rho_Z} \right)^\nu K_\nu \left( \sqrt{2\nu} \frac{r}{\rho_Z} \right), \quad r > 0, \quad (6)$$

with the smoothness parameter  $\nu = 2$  and  $\boldsymbol{\theta}_Z = (\sigma_Z^2, \rho_Z)$ , where  $\sigma_Z^2$  and  $\rho_Z$  are the variance and range parameters, respectively, and  $K_\nu$  is the modified Bessel function of the second kind (see e.g. Cressie, 1993; Chilés and Delfiner, 1999; Banerjee et al., 2004). The choice  $\nu = 2$  was made since we expect that the unobserved environmental conditions that affect the clustering of  $\mathbf{x}$  in our application vary rather smoothly and since it is computationally convenient (Lindgren et al., 2011).

Additional fixed covariate effects, if available, can be added in (5). If the random field  $Z$  is left out of the model, the conditional model is simplified to an inhomogeneous Poisson process.

### 2.3 Replicates

Assume that we have several independent replicated point patterns  $\mathbf{x}_i$ ,  $i = 1, \dots, n$ , from the conditional distribution of the point process  $X$  given  $Y = \mathbf{y}_i$ ,  $i = 1, \dots, n$ . Conditionally on  $Y = \mathbf{y}_i$ , the model for  $\mathbf{x}_i$  is a LGCP with the intensity  $\Lambda(s; \beta_0, \beta_1, \boldsymbol{\theta}_I, \mathbf{y}_i, Z_i)$  in (5), where  $Z_i$ ,  $i = 1, \dots, n$ , are independent replicates of the Gaussian random field with parameters  $\boldsymbol{\theta}_Z$ . In our case, it is not reasonable to assume that all replicates have the same  $\beta_0$ , which controls the number of points of  $X$ , and we let each pattern  $\mathbf{x}_i$  to have its own intercept parameter  $\beta_0$ , i.e.  $\beta_{0i}$  for  $\mathbf{x}_i$ ,  $i = 1, \dots, n$ . Consequently, in our application below, the pattern  $\mathbf{x}_i$  is assumed to be a realization of the LGCP model with the intensity  $\Lambda(s; \beta_{0i}, \beta_1, \boldsymbol{\theta}_I, \mathbf{y}_i, Z_i)$ .

## 3 Inference

The likelihood of the conditional LGCP model for a point pattern  $\mathbf{x}$  with  $n$  points observed in  $W$  is

$$p(\mathbf{x}; \boldsymbol{\beta}, \boldsymbol{\theta}_I, \boldsymbol{\theta}_Z, \mathbf{y}) = \mathbf{E}_{\boldsymbol{\theta}_Z} \prod_{i=1}^n \Lambda(x_i; \boldsymbol{\beta}, \boldsymbol{\theta}_I, \mathbf{y}, Z) \exp \left( - \int_W \Lambda(u; \boldsymbol{\beta}, \boldsymbol{\theta}_I, \mathbf{y}, Z) du \right), \quad (7)$$

where  $\boldsymbol{\beta}$ ,  $\boldsymbol{\theta}_I$ ,  $\boldsymbol{\theta}_Z$  are the model parameters,  $Z$  denotes the Gaussian random field and the expectation is over  $Z$  given  $\boldsymbol{\theta}_Z$ . As we use Bayesian inference we need to be able to evaluate the likelihood (7) efficiently. Below, we describe the approximations needed: discretization of the observation window (Section 3.1), an edge-corrected influence field (Section 3.2), and approximations related to the Gaussian field (Section 3.3), which include approximating the field by a Gaussian Markov random field and using the Laplace approximation to evaluate the likelihood. Finally, the approximated likelihood based

on replicates is given in Section 3.4 and the MCMC algorithm is described in Section 3.5.

### 3.1 Discretization

To be able to make inference on LGCp models, the observation window  $W$  of the point pattern  $\mathbf{x}$  is discretized using a regular grid in a similar manner as in Rue et al. (2009) and Møller et al. (1998). Therefore,  $W$  is divided into  $G$  disjoint cells  $\{w_g\}$  with center locations  $\xi_g$  and each with area  $|w|$ . Furthermore, we let  $n_g^x$  denote the number of points of  $\mathbf{x}$  within  $w_g$  in  $W$  and  $\mathbf{n}^x = (n_1^x, \dots, n_G^x)$ . A piecewise constant approximation is used for the intensity  $\Lambda$  and the Gaussian field  $Z$ , and the locations of  $\mathbf{x}$  are replaced by the counts  $n_g^x$ . The likelihood for  $\mathbf{n}^x$  is

$$p(\mathbf{n}^x; \boldsymbol{\beta}, \boldsymbol{\theta}_I, \boldsymbol{\theta}_Z, \mathbf{y}) = \mathbf{E}_{\boldsymbol{\theta}_Z} p(\mathbf{n}^x; \boldsymbol{\beta}, \boldsymbol{\theta}_I, \mathbf{y}, Z), \quad (8)$$

where

$$p(\mathbf{n}^x; \boldsymbol{\beta}, \boldsymbol{\theta}_I, \mathbf{y}, Z) = \prod_{g=1}^G \frac{(|w| \tilde{\Lambda}(\xi_g; \boldsymbol{\beta}, \boldsymbol{\theta}_I, \mathbf{y}, Z_g))^{n_g^x}}{n_g^x!} \exp(-|w| \tilde{\Lambda}(\xi_g; \boldsymbol{\beta}, \boldsymbol{\theta}_I, \mathbf{y}, Z_g)),$$

where  $Z_g$  is the value of the piecewise approximation of  $Z$  in the grid cell  $g$  and  $\tilde{\Lambda}(\xi_g; \boldsymbol{\beta}, \boldsymbol{\theta}_I, \mathbf{y}, Z_g)$  is the discrete version of (5) which includes dependence on the pattern  $\mathbf{y}$ .

### 3.2 Edge correction

Typically, when Poisson processes or Cox processes are considered, we do not have to pay any specific attention to the edges of the observation window  $W$ . In the conditional case, however, the points of  $Y$  that are outside  $W$  may have an effect on the intensity of  $X$  in  $W$ . Therefore, we propose an imputation type approach, similar to the one proposed by Kühlmann-Berenzon et al. (2005), to correct for the unobserved points of  $Y$ . Assuming that  $Y$  is a homogeneous Poisson process with intensity  $\lambda$ , it then follows that  $Y_{W^c}$ , the process outside  $W$ , is an inhomogeneous Poisson process with intensity  $y \mapsto \lambda \mathbf{1}(y \notin W)$  and independent of the points inside  $W$  and by using the Campbell theorem (see e.g. Chiu et al., 2013) we can write

$$\begin{aligned} \mathbf{E}C(s; \boldsymbol{\theta}_I, Y_{W^c}) &= \mathbf{E} \sum_{[y_j, m_j] \in Y_{W^c}} c(\|s - y_j\|, m_j; \boldsymbol{\theta}_I) \\ &= \int_{R_+} \int_{R^2} c(s - y, m; \boldsymbol{\theta}_I) \mathbf{1}_{W^c}(y) \lambda dy dF(m). \end{aligned}$$

By changing the order of the integrals we find that

$$\begin{aligned}\mathbf{E}C(s; \boldsymbol{\theta}_I, Y_{W^c}) &= \int_{R^2} f(s-y) \mathbf{1}_{W^c}(y) \lambda dy \\ &= \int_{R^2} f(s-y) \lambda dy - \int_{R^2} f(s-y) \mathbf{1}_W(y) \lambda dy,\end{aligned}$$

where  $f(y) = \int_{R_+} c(\|y\|, m; \boldsymbol{\theta}_I) dF(m)$ . By changing to polar coordinates and with a slight abuse of notation

$$\int_{R^2} f(s-y) \lambda dy = \lambda 2\pi \int_0^\infty r f(r) dr,$$

which can be computed using numerical integration. Since we are only interested in locations  $s \in W$ , we can replace the function  $f$  with  $f\mathbf{1}_{W^S}$ , the restriction of  $f$  to the set  $W^S = \{s - y : s \in W, y \in W\}$ , and

$$\int_{R^2} f(s-y) \mathbf{1}_W(y) dy = \int_{R^2} (f\mathbf{1}_{W^S})(s-y) \mathbf{1}_W(y) \lambda dy = (f\mathbf{1}_{W^S} * \mathbf{1}_W)(s).$$

The discrete convolution of the piecewise constant approximations of  $f\mathbf{1}_{W^S}$ , and  $\mathbf{1}_W$  can be efficiently computed using discrete Fourier transforms (Oppenheim et al., 1999; Frigo and Johnson, 2005). For  $F$ , we use the empirical distribution of marks.

The edge-corrected influence field value at any location  $s \in W$  is then obtained as the sum of the influence field calculated from the observed  $\mathbf{y}_W$ ,  $C(s; \boldsymbol{\theta}_I, \mathbf{y}_W)$ , and the expected influence load of the unobserved  $Y_{W^c}$ . In general, we use the numerical approximation explained above but for the special case of the Gaussian influence kernel (2) and a rectangular observation window, it is easy to compute the edge correction by hand.

### 3.3 Approximations related to the Gaussian field

We use Laplace approximation (Tierney and Kadane, 1986; Rue et al., 2009) to approximate the likelihood (8) and obtain

$$\mathbf{E}_{\boldsymbol{\theta}_Z} p(\mathbf{n}^x; \boldsymbol{\beta}, \boldsymbol{\theta}_I, \mathbf{y}, Z) \approx \sqrt{\frac{(2\pi)^d}{\det(-H(\hat{z}))}} p(\mathbf{n}^x; \boldsymbol{\beta}, \boldsymbol{\theta}_I, Y, \hat{z}) p(\hat{z}; \boldsymbol{\theta}_Z), \quad (9)$$

where  $H$  and  $\hat{z}$  are the Hessian and maximizer of  $z \mapsto p(\mathbf{n}^x; \boldsymbol{\beta}, \boldsymbol{\theta}_I, Y, z) p(z; \boldsymbol{\theta}_Z)$ , respectively, and  $p(z; \boldsymbol{\theta}_Z)$  is the probability density of the vector  $Z_1, \dots, Z_G$ .

Since the Gaussian random field  $Z$  is assumed to have mean zero and the Matérn covariance function (6) with  $\nu = 2$ , we can utilize the explicit link

between Gaussian fields and Markov random fields (Lindgren et al., 2011), which tells us that the distribution of  $Z_1, \dots, Z_G$  should be approximated with a Gaussian distribution with a precision matrix given by Lindgren et al. (2011).

### 3.4 Replicates

Since the point patterns are assumed to be conditionally independent, the likelihoods (7) for each replicate can be multiplied to yield the final likelihood

$$p(\mathbf{x}_1, \dots, \mathbf{x}_N; \boldsymbol{\beta}, \boldsymbol{\theta}_I, \boldsymbol{\theta}_Z, Y_1, \dots, Y_N) = \prod_{k=1}^N p(\mathbf{x}_1, \dots, \mathbf{x}_N; \beta_{0i}, \beta_1, \boldsymbol{\theta}_I, Y_k), \quad (10)$$

where now  $\boldsymbol{\beta}$  contains all the regression coefficients, i.e.  $\boldsymbol{\beta} = (\beta_{01}, \dots, \beta_{0N}, \beta_1)$ . To obtain an approximation of (10), the approximations (8) and (9) are applied to each pattern separately.

### 3.5 MCMC

Combining the likelihood (10) with the prior  $p(\boldsymbol{\beta}, \boldsymbol{\theta}_I, \boldsymbol{\theta}_Z)$  yields the posterior

$$p(\boldsymbol{\beta}, \boldsymbol{\theta}_I, \boldsymbol{\theta}_Z; \mathbf{x}_1, \dots, \mathbf{x}_N, Y_1, \dots, Y_N) \propto p(\boldsymbol{\beta}, \boldsymbol{\theta}_I, \boldsymbol{\theta}_Z) p(\mathbf{x}_1, \dots, \mathbf{x}_N; \boldsymbol{\beta}, \boldsymbol{\theta}_I, \boldsymbol{\theta}_Z, Y_1, \dots, Y_N)$$

which is approximated by applying all the above mentioned approximations. To sample from the approximated posterior distribution, we use Robust Adaptive Metropolis algorithm (Vihola, 2012, 2020), which uses a Gaussian random-walk proposal distribution, whose covariance is updated adaptively. The limiting proposal covariance matches the shape of the posterior, such that an average acceptance rate of 0.234 is attained, following the theoretical findings presented e.g. in Roberts et al. (1997).

## 4 Simulation experiment

We made a small simulation experiment to study the performance of the inference approach suggested above and in particular, to compare the estimates of the influence field and random field parameters without any edge correction, with Poisson edge correction and with plus sampling. The plus sampling represents the truth or the ideal situation. The point pattern  $\mathbf{y}$  was a realization either of a Poisson process or a regular Strauss process. The Strauss process (see e.g. Illian et al., 2008) was included to see whether

the edge correction based on the Poisson assumption of  $Y$  would work even in a more regular case. We did not include any cluster process since in our application, the large tree patterns  $\mathbf{y}$  are regular. Also, based on a small simulation study (results not shown here), it is unlikely that the Poisson correction would work well when the  $\mathbf{y}$  pattern is strongly clustered.

#### 4.1 Set-up

The intensity of the Poisson and Strauss processes was chosen such that it results in approximately 60 points in  $W$ . Furthermore, in the Strauss process the interaction strength was 0.1 and interaction radius 2. The  $\mathbf{x}$  patterns were generated on  $W = [0, 40] \times [0, 40]$  and the  $\mathbf{y}$  patterns on the extended window  $W_{\text{ext}} = [-20, 60] \times [-20, 60]$  to be able to use plus sampling. Initially, the parameters of the conditional LGCP model with the Gaussian influence kernel (2), as well as the intensity of  $Y$ , were chosen to correspond approximately to the estimates obtained from one of the data patterns analysed in Section 5, namely the EVO02 pattern, setting them to  $\beta_0 = -1$ ,  $\beta_1 = -1$ , and  $\theta = 2.8$ . In addition, we used the same kernel and either the values  $\beta_0 = -0.4$ ,  $\beta_1 = -3$ , and  $\theta = 2.8$  corresponding to a much stronger effect of the influence kernel ( $\beta_1$ ) or the values  $\beta_0 = 0.6$ ,  $\beta_1 = -1$ , and  $\theta = 5.6$  corresponding to a much larger range of influence  $\theta$  than in EVO02. In all cases,  $\sigma_Z = 1.2$  and  $\rho_Z = 2.8$ . The parameter  $\beta_0$  varied to keep the expected number of points the same in each case.

We fitted the conditional LGCP model above to the simulated point patterns. We discretized the observation windows to pixels of size 1 m  $\times$  1 m and set independent priors for all model parameters as follows: For all the parameters in  $\beta$ , we used independent Gaussian distributions with mean zero and standard deviation 10. For the range parameters  $\rho_Z$  and  $\theta$ , we set the prior to be the Gamma distribution with shape parameter 3 and scale parameter 1. Furthermore, the prior for the standard deviation of the Gaussian field  $\sigma_Z$  was the exponential distribution with expectation 1.

For each point pattern, we then ran the MCMC scheme using a) no edge correction, b) the Poisson edge correction and c) plus sampling edge correction with 100 000 updates using the true parameter values as the starting values.

#### 4.2 Results

An example of the expected intensity field with and without edge correction for the conditional LGCP model with the parameters estimated from the

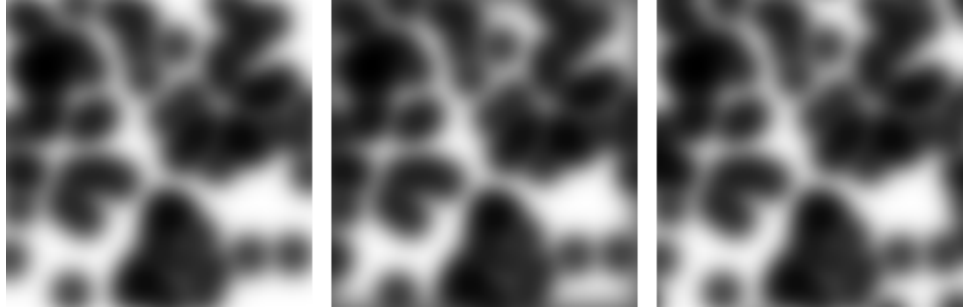


Figure 1: Expected intensity of the conditional LGCP with parameters estimated from the EVO02 pattern using no edge correction (left), Poisson correction (middle) and plus sampling (right). The  $\mathbf{y}$  pattern is a realization of a Strauss process with interaction parameter 0.1, interaction range 2, and with on average 60 points. Dark color means low intensity.

EVO02 pattern and Strauss pattern  $\mathbf{y}$  is shown in Figure 1. It can be seen that the Poisson corrected and the plus sampling corrected intensities are quite similar to each other, see especially the right corners in the middle and right panels. If no edge correction is used (left), the intensity is higher in these corners than in the edge corrected cases (middle and right).

The posterior means of the parameters from the simulation experiment are shown in Figure 2. By looking at the plus sampling corrected estimates, we can see that the approximations used in the estimation led to reasonable results: almost all 95% posterior intervals contained the true values. In particular the influence parameters  $\beta_1$  and  $\theta$  were estimated rather well. The intercept  $\beta_0$  was slightly underestimated when the process  $Y$  was either Poisson or Strauss with wide influence.

Comparing the different edge correction methods, when  $Y$  was a Poisson process, estimates without any correction were approximately as close to the plus sampling corrected estimates as the Poisson corrected estimates were, and the edge correction played a minor role. In the Strauss case, the Poisson corrected estimates tended to be closer to the estimates based on plus sampling than the uncorrected estimates were when the influence of  $\mathbf{y}$  was strong (large negative  $\beta_1$ ) and its range wide (large  $\theta$ ). Including the Poisson edge correction did not have much effect on the quality of the estimate of  $\beta_1$ . However, the estimates of  $\beta_0$  and  $\theta$  obtained using the Poisson edge correction were closer to the plus sampling estimates than the non-corrected estimates were in the case of strong influence or wide influence range. Even the estimates of the parameters of the random field,  $\sigma_Z$  and  $\rho_Z$ ,

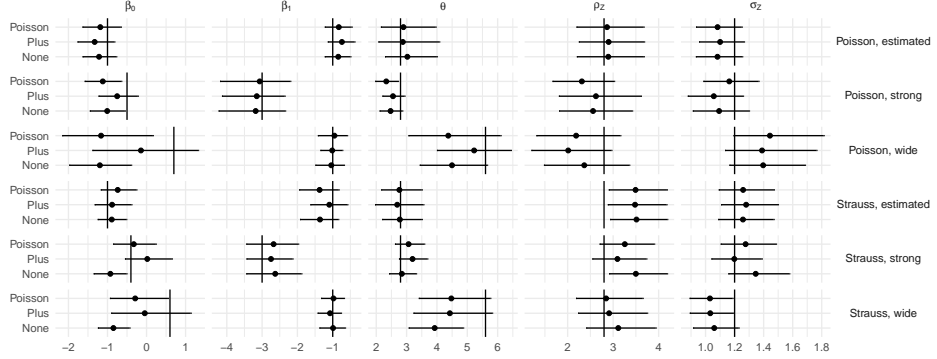


Figure 2: Posterior means (dots) and 95% quantile intervals of the different edge corrected (left column) estimates of the parameters together with the parameter values used in the simulations (vertical lines) for different  $\mathbf{y}$  patterns and different competition effects (right column). The  $\mathbf{y}$  patterns are realizations of a Poisson process or of a Strauss process with interaction strength 0.1 and range 2 (see the left side), both with on average 60 points in the observation window  $W$ . The  $\mathbf{x}$  patterns were generated from the conditional LGCP model with EVO02 parameters (estimated), with stronger influence (strong) and with wider influence range (wide).

improved when the edge correction was used. Thus, in this rather limited simulation study, the Poisson edge correction could improve the estimates if the influence of the  $\mathbf{y}$  points on the intensity of  $X$  was strong or the range of influence wide.

## 5 Application

The data shown in Figure 3 have been collected on  $40 \text{ m} \times 40 \text{ m}$  squares in Evo (EVO) and Vesijako (VES), three in Evo and four in Vesijako, in southern Finland. They are part of a larger data set collected for studies on tree and stand development in managed, uneven-aged Norway spruce forests conducted under the ERIKA research project at the Natural Resources Institute Finland (Eerikäinen et al., 2007; Eerikäinen et al., 2014; Saksa and Valkonen, 2011). Using the conditional LGCP model, we studied the effect of the patterns of "large trees"  $\mathbf{y}_i$  (black circles) to the seedling patterns  $\mathbf{x}_i$  (red crosses). The patterns  $\mathbf{y}_i$  consist of Norway spruces which had a vital crown with no damages and a diameter at breast height (dbh) at least 7

cm in 1991. The seedlings are naturally generated Norway spruce seedlings with height at least 10 cm in 1996 that appeared after the data collection in 1991.

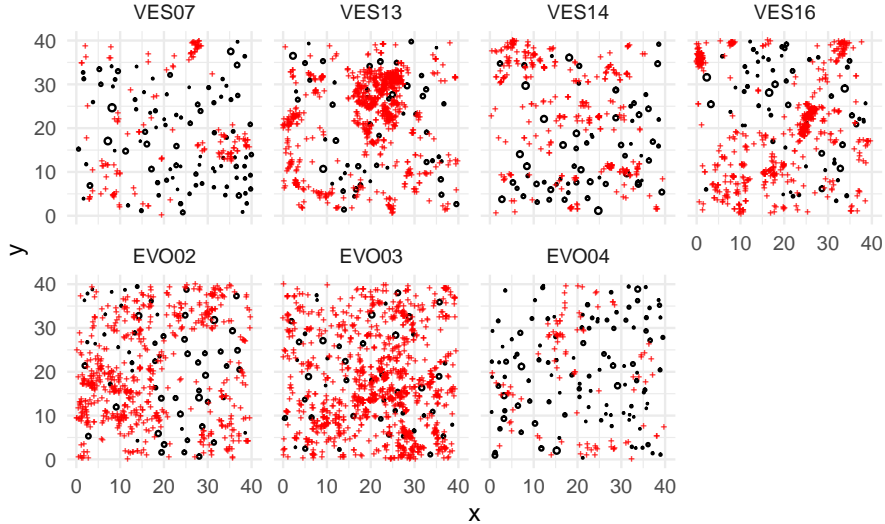


Figure 3: Spruces with dbh at least 7 cm (open circles with radii relative to the dbh of the spruce) and new seedlings (red crosses) in areas of size  $40 \text{ m} \times 40 \text{ m}$  in Vesijako (top) and EVO (bottom).

We first fitted the conditional LGCP model using different alternative influence fields to the pattern EVO02 (results not shown). The model without any influence from the large trees did not fit to the data well. The most appropriate influence kernels were the Gaussian kernels with gradually decreasing influence. However, it was not clear which of the Gaussian kernels, (2) or (4), had the best fit, and therefore, we chose to consider only the simplest one of them, namely the simple Gaussian kernel (2).

Then, we fitted the conditional LGCP model to the two sets of sample plots, EVO and VES, separately. We used the same discretization of the observation window and the same priors as in the simulation experiment (Section 4.1). For both data sets, we then run the MCMC scheme using the Poisson edge correction with 120 000 updates, leaving out the first 20 000 observations of the chains as the burn-in.

Figures 4 and 5 show the marginal posterior distributions for the common model parameters and for the plot specific intercepts, respectively. The influence of the large trees on the seedlings is clearly negative in both data

sets ( $\beta_1 < 0$ ) meaning that the seedlings avoid locations in the close vicinity of the large trees. The variance  $\sigma_Z$  and range  $\rho_Z$  of the random field were estimated clearly larger in VES than in EVO indicating that there is more unexplained variation in VES than in EVO. There is also some indication that the range of influence  $\theta$  is smaller in the VES plots than in the EVO plots, but due to the wide posterior interval in the EVO case, we cannot really conclude that this is the case. The range of influence  $\theta$  of the large trees was estimated to be around 2.1 m in the VES data, indicating that the influence of a large tree decreases from its maximum influence (at the tree location) to 37% of it at distance 2.1 m from the tree. In the EVO data, the posterior mean for  $\theta$  was 2.9 m. As can be seen in Figure 5, having separate intercepts for each sample plot was necessary.

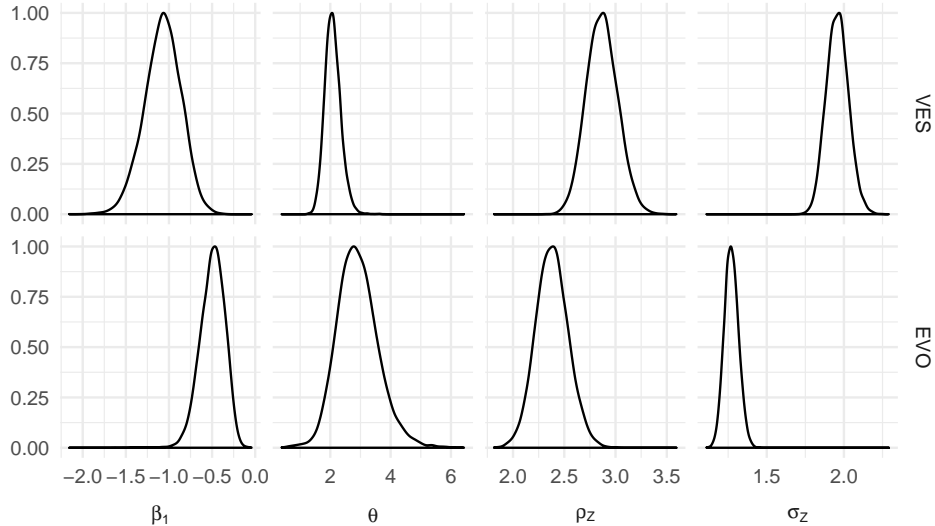


Figure 4: Marginal posterior distributions of the common parameters for VES (top) and EVO (bottom).

To evaluate the goodness-of-fit of the models, we used the posterior predictive model assessment based on various summary characteristics, namely the  $L$ -function (variance stabilizing version of Ripley's  $K$ ), the empty space function  $F$ , and the nearest neighbour distribution function  $G$  summarizing the spatial pattern  $\mathbf{x}$  and, to investigate the relationship between the large trees and seedlings, the cross  $L$ -function,  $L_{12}$  (see e.g. Illian et al., 2008; Diggle, 2013). For each plot, we generated 10 000 patterns of seedlings from the posterior predictive distributions of the conditional LGCP models given the

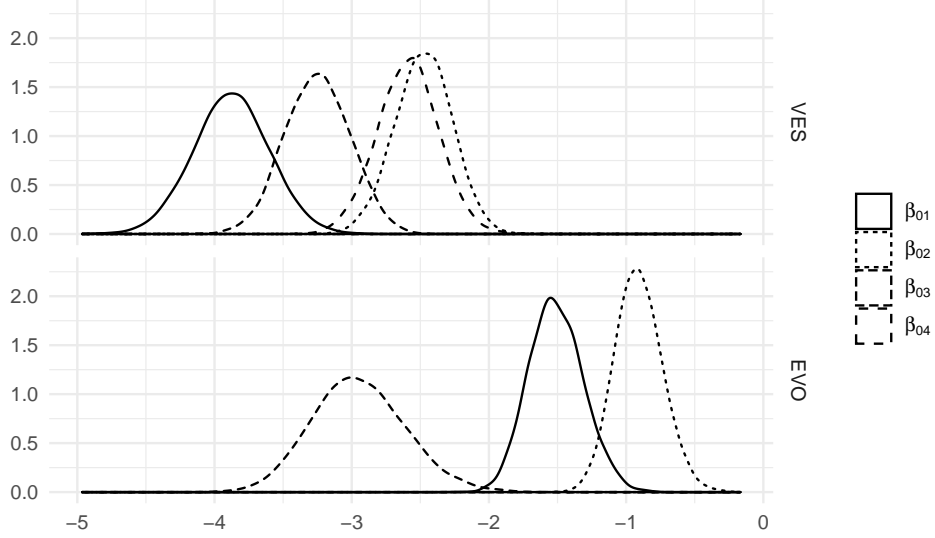


Figure 5: Marginal posterior distributions of the intercept  $\beta_{0i}$  for all seven point patterns.

observed  $\mathbf{y}$  and calculated the summary functions for the data pattern and for each of the generated patterns. Figure 6 shows the 95% global extreme rank length envelopes (Myllymäki et al., 2017; Myllymäki and Mrkvíčka, 2019) constructed from the summary functions based on the fitted model together with the corresponding empirical functions separately for each plot. The fit of the model is reasonably good for all plots. However, for the EVO03 and VES13 patterns we can see some differences between the empirical and simulated functions. Looking at the EVO03 pattern (Figure 3), it seems that the seedling pattern in the top left part of the plot is less clustered than in the bottom right part, and this is not captured by the model (see Figure 7 for simulated realizations of new seedlings). On the other hand, the VES13 pattern has an extraordinary big cluster of seedlings in the middle of the plot, which explains the behavior of the empirical  $L$  and  $L_{12}$  functions at large distances. Further, some deviation from the fitted model is observed in the EVO04 pattern by the nearest neighbor distribution function  $G$  and maybe also by  $L$ , indicating slightly more close pairs of points in the data than in the model simulations.

We further investigated the sensitivity of the results to the chosen priors by performing the same analysis using priors which had double standard deviations in comparison to the initial priors. For Gamma distribution,

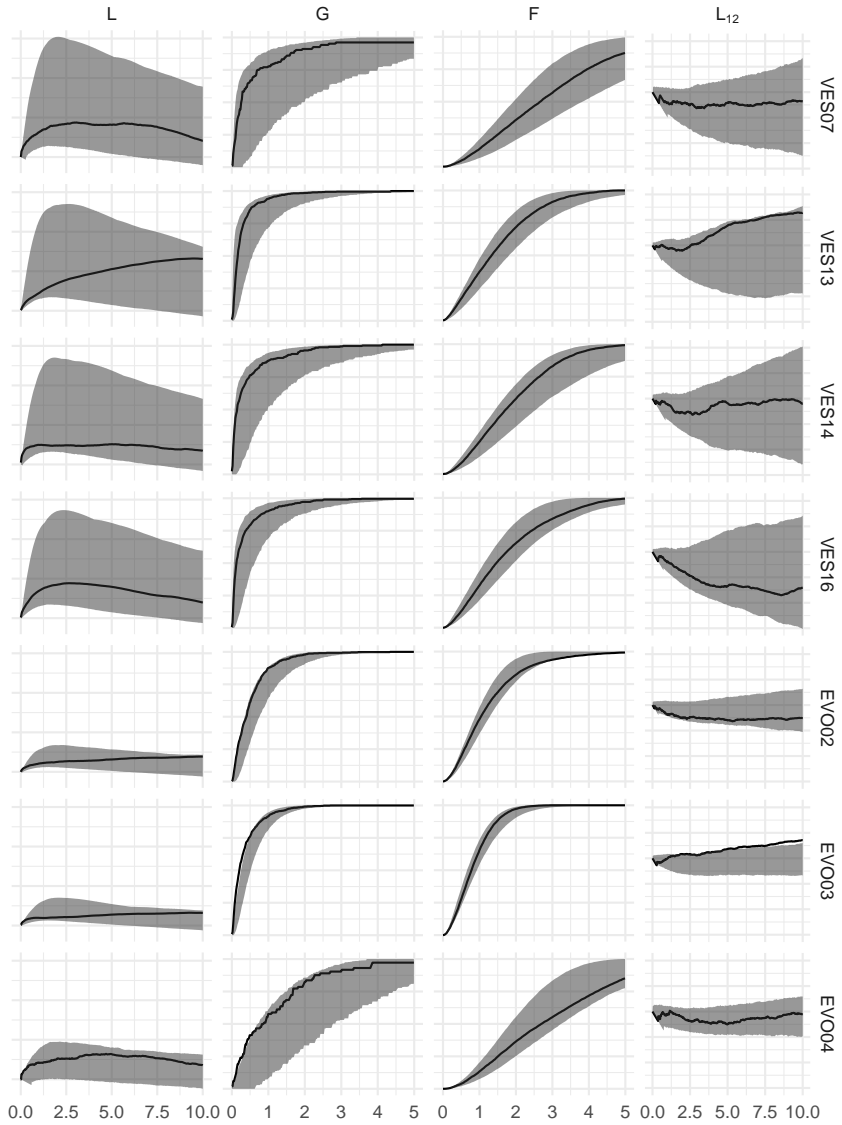


Figure 6: From left to right, the empirical  $L$ ,  $G$ ,  $F$ , and  $L_{12}$  functions (solid lines) together with the 95% global envelopes (grey areas) constructed from 10 000 simulations from the posterior predictive distribution of the fitted conditional LGCP models for the seven plots in Figure 3.

this was achieved by multiplying the scale by four and dividing the shape

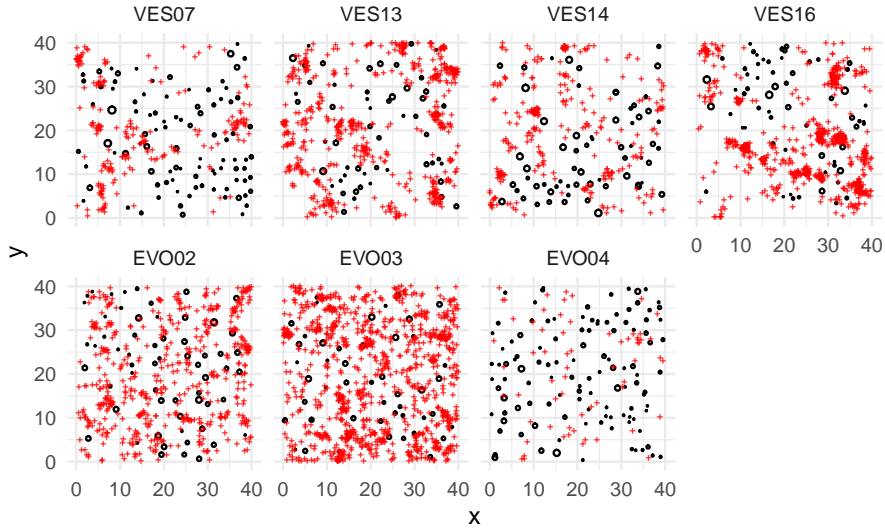


Figure 7: Spruces with dbh at least 7 cm (open circles with radii relative to the dbh of the spruce) and realizations of new seedlings from the fitted models (red crosses) in areas of size 40 m  $\times$  40 m in Vesijako (top) and Evo (bottom).

parameter by four. The change in priors caused only a minor change in the posterior distributions, namely the difference of the means was always less than 0.05.

## 6 Discussion

We introduced a conditional version of the log-Gaussian Cox process to model the effect of some dominating points on the intensity of the remaining points. Particularly, we modeled the intensity of seedlings given the locations and influence kernels of large trees. For parameter estimation, a Bayesian approach using MCMC, Laplace approximation, and replicated point patterns as data was suggested. All computations were implemented in Julia language (Bezanson et al., 2017), while graphics were done using ggplot2 (Wickham, 2016).

We could have defined our model in the R package INLA (Rue et al., 2009) using the `rgeneric` class of models (personal communication with Håvard Rue). A comparison between INLA and MCMC with Laplace ap-

proximation would be interesting since the Laplace approximation that we used for the (marginal) likelihood in (9) is the same as the one used in INLA. However, while trying to define the model in INLA, we encountered some computational difficulties and decided that such a comparison would be out of the scope of this paper.

Since the dominating point pattern  $\mathbf{y}$  outside the sampling window may affect the intensity of the suppressed point pattern  $\mathbf{x}$  within the window, an edge correction based on a Poisson assumption of the dominating point process was included in the estimation procedure. We demonstrated by a small simulation study that this edge correction can improve the parameter estimates when the dominating point process is regular and the effect of the dominating points is rather strong or the range of influence wide. Ideas from Geyer (1999) or Gabriel et al. (2017) could be used to find alternative edge correction methods. In our forestry data, the effect of large trees on the seedlings was not very strong and therefore, the edge correction played only a minor role.

We used the conditional model to understand the tree regeneration in managed, uneven-aged forests. Similar models could be useful even for natural (see e.g. Abellanas and Pérez-Moreno, 2018) or urban forests (Hauru et al., 2012). Our analysis suggests that tree regeneration is affected by the pattern of large trees in the studied data. The conditional model could, therefore, be further used in an experimental setup, where realizations of seedlings were generated for different patterns  $\mathbf{y}$  and the regeneration evaluated by, e.g. some spatial summary function such as the empty space function. Also, the effect of different thinning strategies on regeneration of trees could be evaluated in a similar manner.

## Acknowledgements

MK, MM and MV were financially supported by the Academy of Finland (Project Numbers 306875, 295100 and 315619) and AS by the Swedish Research Council (VR 2013-5212) and the Swedish Foundation for Strategic Research (SSF AM13-0066). The authors thank Helena Henttonen, Jari Hynynen and Sauli Valkonen (Luke) for discussions on the application, and Antti Penttinen for his comments on an earlier version of the manuscript. Further, the authors are grateful to Hilkka Ollikainen and Juhani Korhonen, who mastered the maintenance and measurements on the plots of the ERIKA data set.

## References

Abellanas, B. and P. Pérez-Moreno (2018). Assessing spatial dynamics of a *pinus nigra* subsp. *salzmannii* natural stand combining point and polygon patterns analysis. *Forest Ecology and Management* 424, 136–153.

Adler, F. (1996). A model of self-thinning through local competition. In *Proceedings of the National Academy of Sciences of the United States of America*, Volume 93, pp. 9980–9984.

Banerjee, S., B. P. Carlin, and A. E. Gelfand (2004, December). *Hierarchical Modeling and Analysis for Spatial Data* (1 ed.). Number 101 in Monographs on Statistics and Applied Probability. Boca Raton: Chapman & Hall/CRC.

Bezanson, J., A. Edelman, S. Karpinski, and V. B. Shah (2017). Julia: A fresh approach to numerical computing. *SIAM Review* 59(1), 65–98.

Chilés, J.-P. and P. Delfiner (1999). *Geostatistics: Modeling Spatial Uncertainty*. New York: Wiley.

Chiu, S. N., D. Stoyan, W. S. Kendall, and J. Mecke (2013). *Stochastic Geometry and its Applications* (3 ed.). Chichester: Wiley.

Cressie, N. A. C. (1993, January). *Statistics for Spatial Data* (Revised ed.). Wiley Series in Probability and Mathematical Statistics. New York: Wiley.

Dieckmann, U., R. Law, and J. Metz (Eds.) (2000). *The Geometry of Ecological Interactions: Simplifying Spatial Complexity*. Cambridge Studies in Adaptive Dynamics. Cambridge University Press.

Diggle, P. J. (2013). *Statistical Analysis of Spatial and Spatio-Temporal Point Patterns* (3 ed.). Boca Raton: CRC Press.

Eerikäinen, K., S. Valkonen, and T. Saksa (2014). Ingrowth, survival and height growth of small trees in uneven-aged *picea abies* stands in southern finland. *Forest Ecosystems* 1:5.

Eerikäinen, K., J. Miina, and S. Valkonen (2007). Models for the regeneration establishment and the development of established seedlings in uneven-aged, norway spruce dominated forest stands of southern finland. *Forest Ecology and Management* 242(2), 444–461.

Frigo, M. and S. G. Johnson (2005). The design and implementation of FFTW3. *Proceedings of the IEEE* 93(2), 216–231. Special issue on “Program Generation, Optimization, and Platform Adaptation”.

Gabriel, E., J. Coville, and J. Chadoeuf (2017). Estimating the intensity function of spatial point processes outside the observation window. *Spatial Statistics* 22, 225–239. Spatio-temporal Statistical Methods in Environmental and Biometrical Problems.

Genet, A., P. Grabarnik, O. Sekretenko, and D. Pothier (2014). Incorporating the mechanisms underlying inter-tree competition into a random point process model to improve spatial tree pattern analysis in forestry. *Ecological Modelling* 288, 143–154.

Geyer, C. (1999). Likelihood inference for spatial point processes: Likelihood and computation. In W. Kendall, O. Barndroff-Nielsen, and M. van Lieshout (Eds.), *Stochastic Geometry*, pp. 141–172. Chapman and Hall/CRC.

Grabarnik, P. and A. Särkkä (2009, May). Modelling the spatial structure of forest stands by multivariate point processes with hierarchical interactions. *Ecological Modelling* 220(9–10), 1232–1240.

Hauru, K., A. Niemi, and S. Lehvävirta (2012). Spatial distribution of saplings in heavily worn urban forests: Implications for regeneration and management. *Urban Forestry & Urban Greening* 11(3), 279–289.

Högmander, H. and A. Särkkä (1999). Multitype spatial point patterns with hierarchical interactions. *Biometrics* 55(4), 1051–1058.

Illian, J., A. Penttinen, H. Stoyan, and D. Stoyan (2008). *Statistical Analysis and Modelling of Spatial Point Patterns* (1 ed.). Statistics in Practice. Chichester: John Wiley & Sons, Ltd.

Illian, J. B., J. Møller, and R. P. Waagepetersen (2009, Sep). Hierarchical spatial point process analysis for a plant community with high biodiversity. *Environmental and Ecological Statistics* 16(3), 389–405.

Kühlmann-Berenzon, S., J. Heikkinen, and A. Särkkä (2005, 08). An additive edge correction for the influence potential of trees. *Biometrical journal. Biometrische Zeitschrift* 47, 517–526.

Lindgren, F., H. Rue, and J. Lindström (2011). An explicit link between Gaussian fields and Gaussian Markov random fields: the stochastic partial differential equation approach. *Journal of the Royal Statistical Society: Series B (Statistical Methodology)* 73(4), 423–498.

Miina, J. and T. Pukkala (2002). Application of ecological field theory in distance-dependent growth modelling. *Forest Ecology and Management* 161(1), 101–107.

Møller, J., A. R. Syversveen, and R. P. Waagepetersen (1998). Log Gaussian Cox processes. *Scandinavian Journal of Statistics* 25(3), 451–482.

Møller, J. and R. P. Waagepetersen (2003, September). *Statistical Inference and Simulation for Spatial Point Processes* (1 ed.). Number 100 in Monographs on Statistics and Applied Probability. Chapman & Hall/CRC.

Myllymäki, M. and T. Mrkvička (2019). GET: Global envelopes in R. arXiv:1911.06583 [stat.ME].

Myllymäki, M., T. Mrkvička, H. Seijo, P. Grabarnik, and U. Hahn (2017). Global envelope tests for spatial processes. *Journal of the Royal Statistical Society: Series B (Statistical Methodology)* (79), 381–404.

Oppenheim, A. V., R. W. Schafer, and J. R. Buck (1999). *Discrete-Time Signal Processing* (2nd Ed.). USA: Prentice-Hall, Inc.

Penttinen, A. and A. Niemi (2007). On statistical inference for the random set generated cox process with set-marking. *Biometrical Journal* 49(2), 197–213.

Pommerening, A., A. C. Gonçalves, and R. Rodríguez-Soalleiro (2011). Species mingling and diameter differentiation as second-order characteristics. *Allgemeine Forst- und Jagdzeitung* 182(7/8), 115–129.

Pommerening, A., V. LeMay, and D. Stoyan (2011). Model-based analysis of the influence of ecological processes on forest point pattern formation – A case study. *Ecological Modelling* 222(3), 666–678.

Pommerening, A. and K. Maleki (2014). Differences between competition kernels and traditional size-ratio based competition indices used in forest ecology. *Forest Ecology and Management* 331, 135–143.

Roberts, G. O., A. Gelman, and W. R. Gilks (1997, 02). Weak convergence and optimal scaling of random walk metropolis algorithms. *Ann. Appl. Probab.* 7(1), 110–120.

Rue, H., S. Martino, and N. Chopin (2009). Approximate Bayesian inference for latent Gaussian models using integrated nested Laplace approximations (with discussion). *Journal of the Royal Statistical Society, Series B* 71, 319–392.

Saksa, T. and S. Valkonen (2011). Dynamics of seedling establishment and survival in uneven-aged boreal forests. *Forest Ecology and Management* 261(8), 1409–1414.

Schneider, M. K., R. Law, and J. B. Illian (2006). Quantification of neighbourhood-dependent plant growth by Bayesian hierarchical modelling. *Journal of Ecology* 94(2), 310–321.

Tierney, L. and J. B. Kadane (1986). Accurate approximations for posterior moments and marginal densities. *Journal of the American Statistical Association* 81(393), 82–86.

Vihola, M. (2012). Robust adaptive Metropolis algorithm with coerced acceptance rate. *Statistics and Computing* 22, 997–1008.

Vihola, M. (2020). Ergonomic and reliable Bayesian inference with adaptive Markov chain Monte Carlo. In W. W. Piegorsch, R. Levine, H. H. Zhang, and T. C. M. Lee (Eds.), *Handbook of Computational Statistics and Data Science*. Wiley. to appear.

Wickham, H. (2016). *ggplot2: Elegant Graphics for Data Analysis*. Springer-Verlag New York.

Wu, H.-I., P. J. Sharpe, J. Walker, and L. K. Penridge (1985). Ecological field theory: A spatial analysis of resource interference among plants. *Ecological Modelling* 29(1), 215–243.